applied sciences

MDPI

Review

Ultrafast Optical Control of Magnetic Interactions in Carrier-Density-Controlled Ferromagnetic Semiconductors

Masakazu Matsubara

Department of Physics, Tohoku University, Sendai 980-8578, Japan; m-matsubara@m.tohoku.ac.jp; Tel.: +81-22-795-6421

Received: 8 January 2019; Accepted: 1 March 2019; Published: 6 March 2019

Abstract: Investigation of the interaction of ultrashort laser pulses with magnetically ordered materials has become a fascinating research topic in modern magnetism. Especially, the control of magnetic order by sub-ps laser pulses has become a fundamentally important topic with a high potential for future spintronics applications. This paper will review the recent success in optically controlling the magnetic interactions in carrier-density-controlled ferromagnetic semiconductor EuO doped with Gd ions. When the Gd concentration is low, the magnitude of the magnetic interaction is enhanced by the irradiation of ultrashort laser pulses, whereas it is attenuated when the Gd concentration is high. In ferromagnetic $Eu_{1-x}Gd_xO$, we thereby demonstrate the strengthening as well as the weakening of the magnetic interaction by 10% and within 3 ps by optically controlling the magnetic exchange interaction. This principle—ultrafast optical control of magnetic interaction—can be applied to future ultrafast opto-spintronics.

Keywords: ultrafast spin control; opto-spintronics; exchange interaction; europium oxide; ferromagnetic semiconductor; nonlinear magneto-optics; pump-probe spectroscopy

1. Introduction

Spintronics, also known as spin-electronics, utilizing the spin degree of freedom in addition to the charge of electrons has attracted much attention in recent years from the viewpoint of the creation of new driving principles of electric and magnetic devices and energy conservation technology. While technical innovation in conventional semiconductor technology is approaching its limit, spintronics can open new paths to further development and will create new devices that exceed the limitations of conventional ones [1]. The important element in their development is how efficiently one can control the electron spin. Up until now, magnetic fields have been used as the most popular method for controlling the electron spin (or the magnetization of a magnetic material). In recent years, however, alternative methods such as a spin polarized current, an electric field, and a pure spin current, which are in principle not accompanied by Joule heating, are attracting much attention from the viewpoint of low power consumption spin control.

On the other hand, the demand for an ever-increasing speed of manipulation in magnetic information storage has triggered a search for new methods for control of the spin functionality on the ultrafast timescale. Since the control speed of the spin by magnetic fields is already approaching its limit, how fast the spin functionality can be manipulated is one of the most important issues in modern technology. Under such circumstances, the recent development of ultrafast optical technology has opened the way to control the spin by light. In particular, the use of ultrashort optical pulses that are much shorter than the fundamental timescales such as spin-lattice relaxation or precession times allows us to excite magnetic media and to study the spin dynamics after ultrashort optical

excitations. These new possibilities have recently led to exciting results demonstrating changes in the spin state on a sub-ps timescale [2]. For example, by the irradiation of ∼100 fs laser pulse with various pulse shapes, ultrafast demagnetization in ferromagnetic metals [3–6], magnetization reversal in ferrimagnetic (ferromagnetic) alloys [7,8], enhancement of magnetization in magnetic semiconductors [9,10], generation of ferromagnetic order in strongly correlated electron systems [11], and generation and control of spin waves in magnetic insulators [12] have been realized. In the first place, in order to control the spin functionality on the ultrafast timescale, a strong magnetic interaction of the large energy scale (effective magnetic field acting on spins) should be utilized. Therefore, the use of exchange interaction or spin-orbit interaction might be desired for that purpose (Figure 1).

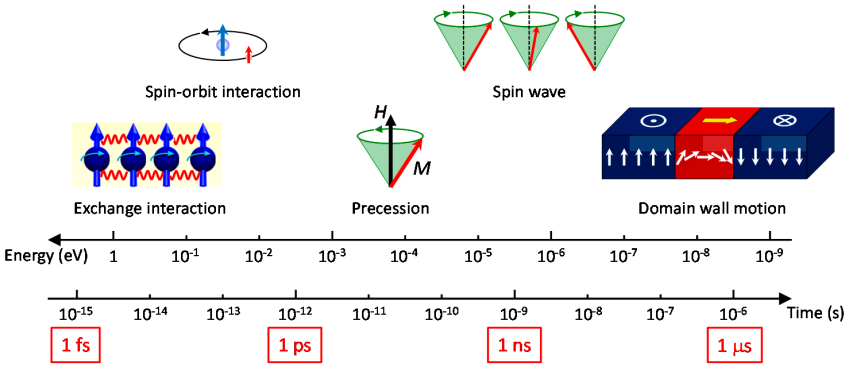

Figure 1. Characteristic energy and timescales of various magnetic phenomena. Timescales t are determined by the interaction energies E via the Heisenberg relation $t = h/E$ (t(fs) $\sim$ 4.13/E(eV)). Here, $h = 4.13 \times 10^{-15}$ eV·s is Planck's constant. The slowest dynamics is the domain-wall motion whose typical timescale is few ns to hundred μs. Precession of magnetization occurs within 10–100 ps and gets damped in sub-ns to tens of ns. Thus, the spin waves in ferromagnetic materials can propagate within few hundreds of ps to tens of ns before it gets damped out. Elementary interactions in magnetism such as the spin-orbit interaction (∼10 fs–1 ps) and the exchange interaction (∼10 fs) are related to faster dynamics.

In this review paper, I will show that ultrafast strengthening or quenching of the ferromagnetic order can be achieved via resonant photoexcitation in carrier-density-controlled ferromagnetic semiconductor EuO doped with Gd ions ($Eu_{1-x}Gd_xO$) [13]. The change of the magnetic order is established within 3 ps and detected by nonlinear magneto-optical effects. Such spin dynamics cannot be explained by a well-known three-temperature model. The associated spin dynamics is explained by the interplay of chemically and optically generated carriers and the resulting dynamic renormalization of the Ruderman-Kittel-Kasuya-Yoshida (RKKY)-like magnetic exchange coupling. The change from ultrafast enhancement to quenching of ferromagnetism is marked by the crossover from the predominantly semiconducting to the predominantly metallic doping range of $Eu_{1-x}Gd_xO$. Aside from the generalized insight into ultrafast spin as well as charge dynamics, a key requirement for spintronics technology, our investigation provides guiding information for the selection and design of materials for ultrafast optical control of magnetic interactions.

2. Ferromagnetic Semiconductor EuO

The target material for this study is europium oxide (EuO) which is known as a representative ferromagnetic semiconductor. EuO, more generally, europium chalcogenides EuX (X = O, S, Se, and Te), have long been attracting attention since its discovery in 1960s as magnetic semiconductors that possess both the electrical properties of semiconductors and the magnetic properties of magnets [14,15]. Recently, a multitude of extreme properties in EuO (or slightly carrier doped EuO) such as nearly 100% spin polarization in the ferromagnetic state [16–18], drastic insulator-metal transition [19], colossal magnetoresistance [20,21], pronounced linear and nonlinear magneto-optical effects [22–26],

theoretical prediction of strain-induced ferroelectricity [27] have been attracting much attention from the viewpoint of basic science and application. In fact, its structural and electronic compatibility with Si, GaN, and GaAs make EuO a very attractive candidate for future semiconductor-based spintronics applications [28–30]. In the past, it was difficult to precisely control the sample quality due to undesirable oxidation and defects. With the recent developments of thin film fabrication technology, however, it is now possible to prepare high quality EuO films with well-controlled carrier density [31].

Undoped EuO is a typical Heisenberg ferromagnet with the Curie temperature T_C of 69 K. The Eu^{2+} ions on a centrosymmetric cubic rock salt structure (Figure 2a) have strongly localized $4f^7$ electrons with ${}^8S_{7/2}$ as the ground state ($S = 7/2, L = 0$) and the saturation magnetic moment as large as 7 μ_B arises from the $4f^7$ spins. Due to the strong localization of the $4f$ shell, the direct $4f$–$4f$ exchange interaction with the nearest Eu^{2+} neighbors is not enough to explain the T_C of EuO. Instead, it has been predicted that the ferromagnetic order is driven by a virtual exchange mechanism [32]. According to this model, localized $4f$ electrons are virtually excited into the empty $5d$ orbital and create virtual magnetic excitons, and the excited $5d$ electron undergoes the intra-atomic $4f$–$5d$ exchange interaction with $4f$ spins at the adjacent sites so that the magnetic exchange coupling J_{ex} can be mediated via the spatially more extended $5d$ orbitals (Figure 2b). This indirect exchange interaction is considered to be stronger than the direct one. Therefore, it should be able to enhance the exchange interaction by truly populating the $5d$ orbitals.

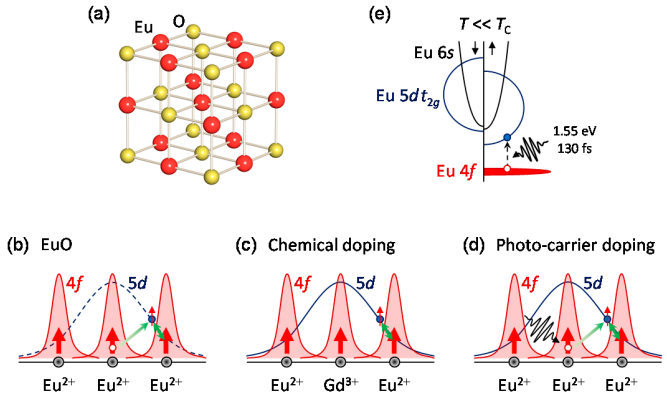

Figure 2. (**a**) Crystal structure of EuO. (**b**) Exchange interaction in undoped EuO via virtual $4f$–$5d$ excitation. (**c**) Introduction of $5d$ electrons by chemical doping. (**d**) Introduction of $5d$ electrons by $4f$–$5d$ photoexcitation. (**e**) Schematic of the spin- and energy-dependent density of states of undoped EuO below T_C and the introduction of $5d$ electrons by resonant $4f$–$5d$ photoexcitation.

A typical way to enhance the exchange interaction is the introduction of carriers by chemical doping [31,33]. For example, by substituting a part of Eu^{2+} ions (Eu^{2+}: [Xe] $4f^7$) with magnetically equivalent Gd^{3+} ions (Gd^{3+}: [Xe] $4f^7$), spatially spread excess $5d$ electrons are introduced and expected to enhance the exchange interaction (Figure 2c). Indeed, the magnetic properties of EuO drastically change by the Gd doping (Figure 3a) and it has been clarified that the increase in the carrier density n_c due to the Gd doping leads to the increase of the exchange interaction J_{ex} and as a result the increase in T_C (Figure 3b). Note that these dopant electrons do not form excitons, but rather occupy the Gd $5d$ impurity orbitals, which in the metallic phase below T_C merge with the Eu $5d/6s$ conduction band to produce a long-range RKKY contribution to J_{ex}.

Control of the exchange interaction should be possible even by photo-carrier doping (Figure 2d). In undoped EuO, there is a band gap (~1.2 eV at room temperature) between the Eu $4f$ orbital and the Eu $5d/6s$ orbital, and the $4f$–$5d$ exchange interaction splits the $5d/6s$ orbital below T_C (Figure 2e). This situation raises the exciting possibility that an ultrafast enhancement of the exchange interaction J_{ex} may be driven by resonant optical pumping of electrons from the Eu $4f^7$ ground state to the $4f^6 5d\left(t_{2g}\right)$ magnetic exciton state (Figure 2e), since this turns the virtual magnetic exciton into a real

one, promoting the magnetic order. In this way, the photoinduced charge dynamics results in an effective time-dependent magnetic coupling between the Eu $4f$ moments. Thus, the investigation of photo-carrier doping effect into EuO is expected to provide a suitable stage for studying the ultrafast optical control of magnetic interactions.

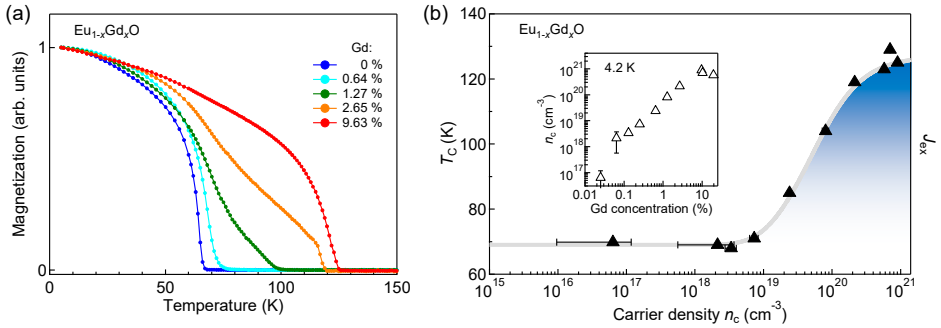

Figure 3. Changes in static magnetic properties of ferromagnetic semiconductor $Eu_{1-x}Gd_xO$ films by carrier doping [31]. (**a**) Temperature dependence of the magnetization in $Eu_{1-x}Gd_xO$ for some characteristic Gd concentrations. (**b**) Carrier density n_c dependence of the Curie temperature T_C. The inset shows the relation between Gd concentration and carrier density n_c.

3. Experiments

Previous experiments on undoped EuO showed that the static conductivity was increased by the irradiation of continuous laser beam [34] and the dynamic enhancement of magnetization by ultrashort laser pulses was possible as demonstrated by means of time-resolved Faraday rotation [35]. In addition, it has been reported that the spin orientation can be controlled by circularly polarized optical pulses via the inverse Faraday effect in EuO [36] and EuTe [37], and the ultrafast dynamics and modulation of the exchange interaction can be accessed using an all-optical technique in EuTe [38]. In this study, ultrafast spin dynamics after the photoexcitation were investigated in carrier-density-controlled ferromagnetic semiconductor $Eu_{1-x}Gd_xO$ films by using a pump-probe nonlinear magneto-optical spectroscopy [39–42] (Figure 4a), as described below.

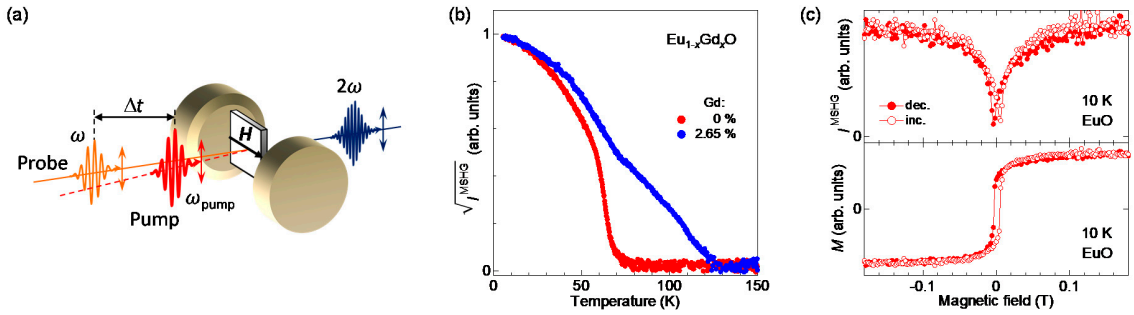

Figure 4. (**a**) Schematic representation of pump-probe nonlinear magneto-optical spectroscopy used in this study. The sample is excited by the pump pulse and the pump-induced changes in magnetic properties are detected by the probe pulse by using magnetization-induced second harmonic generation (MSHG). (**b**) Temperature dependence of the square root of the static MSHG intensity $\sqrt{I^{\mathrm{MSHG}}}$ for undoped and 2.65% Gd-doped EuO (without pump irradiation). (**c**) The upper panel shows magnetic-field dependence of the MSHG intensity at 10 K in undoped EuO. Data represented by closed and open symbols were taken with decreasing and increasing fields, respectively. The lower panel shows magnetization curve extracted from the data in the upper panel.

3.1. Sample Preparation

Epitaxial $Eu_{1-x}Gd_xO(001)$ films (x = 0–19.5%) with a thickness of ~35 nm were grown under adsorption-controlled conditions on double-side-polished $YAlO_3(110)$ single-crystal substrates by

molecular-beam epitaxy. The films were protected against air by an amorphous silicon (a-Si) capping layer with 10–20 nm in thickness and found to be free of oxygen vacancies within the resolution limit of X-ray absorption spectroscopy. Uniform growth without secondary phases was confirmed by X-ray diffraction, and the Gd concentration x was determined by prompt-gamma activation analysis and X-ray absorption spectroscopy. The carrier density n_c was estimated by Hall measurements and a sharp rise in T_C was observed at $n_c \sim 1 \times 10^{19}$ cm^{-3} (Figure 3b). All $Eu_{1-x}Gd_xO$ films possess an in-plane magnetic easy axis. Their physical properties were reported in detail in Ref. [31].

3.2. Pump-Probe Nonlinear Magneto-Optical Spectroscopy

3.2.1. Magnetization-Induced Second Harmonic Generation

Static and photoexcited magnetic properties of $Eu_{1-x}Gd_xO$ films were investigated by using nonlinear optical techniques, especially optical second harmonic generation (SHG). Nonlinear optical effects are associated with higher order optical susceptibilities and SHG, the frequency doubling of a light wave in a material, is one of the simplest second-order nonlinear optical effects.

In the majority of cases, SHG is applied to non-centrosymmetric materials or to the surface or interface of centrosymmetric materials where the space inversion symmetry is locally broken and the strongest interaction by the electric-dipole transitions is expected [43–45]. An electromagnetic light field $\boldsymbol{E}$ at frequency ω is incident on a crystal, inducing an oscillation of electric polarization $\boldsymbol{P}$ at frequency 2ω, which acts as a source of a frequency-doubled light wave. This is expressed by:

$$P_i(2\omega) = \varepsilon_0 \chi^{(2)}_{ijk} E_j(\omega) E_k(\omega), \tag{1}$$

with χ as the second-order nonlinear susceptibility and $I^{\mathrm{SHG}} \propto |\boldsymbol{P}(2\omega)|^2$ as intensity of the emitted SHG wave. Following the Neumann principle, symmetry determines the set of tensor components $\chi^{(2)}_{ijk} \neq 0$ [46].

In centrosymmetric systems such as EuO, SHG is only allowed if higher-order multipole contributions in the expansion of the electromagnetic field such as magnetic-dipole or electric-quadrupole contributions are involved [47]. In magnetic semiconductor EuX, this leads to [24,25,48–50]:

$$P_i(2\omega) = \varepsilon_0 \left(\chi^{(i)}_{ijk} + \chi^{(c)}_{ijk} \right) E_j(\omega) H_k(\omega), \tag{2}$$

where the time-invariant (i-type) tensor $\chi^{(i)}_{ijk}$ and the time-noninvariant (c-type) tensor $\chi^{(c)}_{ijk}$ are the second-order nonlinear susceptibilities related to, in the leading order, crystallographic SHG and magnetization-induced SHG (MSHG), respectively. $E_j(\omega)$ and $H_k(\omega)$ in Equation (2) denote the j-polarized electric field and the k-polarized magnetic field of the fundamental light, respectively, that induce the i-polarized SHG wave $P_i(2\omega)$.

For the SHG measurements in this study, the orientation of the samples was chosen such that crystallographic contributions ($\chi^{(i)}_{ijk}$ tensors) to the SHG signal are suppressed so that the coupling to the magnetic order occurs free of background [24,46]. For this purpose, the $Eu_{1-x}Gd_xO$ films are probed with light incident along one of the principal axes ($k \parallel z$) with the spontaneous magnetization parallel to the x (y) direction. In this configuration, any i-type magnetic-dipole SHG are forbidden so that it is expected that the SHG signal has a purely magnetic origin. In this case, the MSHG intensity I^{MSHG} is written by:

$$I^{\mathrm{MSHG}} \propto (J_{\mathrm{ex}} \cdot M)^2, \tag{3}$$

which is proportional to the square of the exchange interaction J_{ex} and the magnetization M [13]. The MSHG signal was measured in a normal-incidence transmission geometry under an in-plane magnetic field of 50 mT, which was applied to sustain a single-domain magnetic state, and separated from the incident fundamental light by short-pass filters and a monochromator and detected with a photomultiplier tube.

It is known that EuO shows a large temperature-dependent spectral shift of the absorption due to the exchange splitting between the spin-up and spin-down states of the 5*d* orbitals [51]. Previous experiments revealed [24] that at $2\hbar\omega = 2.60$ eV, the interference by temperature-dependent linear absorption effects is avoided. We therefore chose it as the MSHG probe energy. Although SHG in the electric-dipole approximation is forbidden in EuO due to the centrosymmetry as mentioned above, pronounced MSHG signals are observed (Figure 4b). The obtained MSHG signal well reflects the magnetic properties of the samples and disappears exactly at T_C, which confirms its purely magnetic origin. Neither crystallographic SHG from the $Eu_{1-x}Gd_xO$ film nor SHG from the a-Si capping layer and the $YAlO_3$ substrate contribute to the net signal, which reveals SHG to be a background-free probe of the magnetic state of the $Eu_{1-x}Gd_xO$ in the a-Si/$Eu_{1-x}Gd_xO$/$YAlO_3$ heterostructure. This contrasts with the results on EuSe and EuTe films grown on BaF_2 substrates where SHG signals not coupling to the magnetic order were present, presumably because of the (111) orientation of the corresponding films [48,49].

The MSHG signal coupling linearly to the magnetization can be also seen in the magnetic field measurements. The upper panel of Figure 4c shows the magnetic field dependence of the MSHG intensity at 10 K in undoped EuO. The MSHG intensity varies by one order of magnitude with the change of magnetic field. Different minima in field increasing and decreasing runs lead to a butterfly shape. Considering that the MSHG intensity is proportional to the square of the magnetization, the dependence of the magnetization on the applied magnetic field is extracted and shown in the lower panel of Figure 4c. The result reveals a pronounced hysteresis and reproduces direct magnetization measurements.

3.2.2. Time-Resolved Magnetization-Induced Second Harmonic Generation

The experimental pump-probe set-up is shown in Figure 4a. The output of a Ti:sapphire regenerative amplifier system at 800 nm (1.55 eV) with a pulse width of $\sim$ 130 fs and a repetition rate of 1 kHz was divided into two beams. One beam was used for resonant pumping of the $4f^7$–$4f^6 5d\left(t_{2g}\right)$ transition at 1.55 eV (Figure 2e). The absorption length of EuO at this photon energy is $\sim$100 nm so that the entire film was excited. The other beam was introduced into an optical parametric amplifier and the output was frequency-converted to 954 nm (1.30 eV). This light was used for probing the time evolution of the ferromagnetic order by MSHG at 477 nm (2.60 eV). By tuning the time delay Δt between the pump pulse and the probe pulse, ultrafast spin dynamics caused by the resonant optical pumping can be measured.

3.3. Experimental Results

3.3.1. General Properties of Photoinduced Spin Dynamics

First, typical results of the photoinduced spin dynamics are presented and its microscopic mechanism will be discussed. Figure 5a shows a time evolution of the photoinduced change of the MSHG intensity normalized by the value before photoexcitation, $\frac{\Delta I^{\mathrm{MSHG}}}{I^{\mathrm{MSHG}}} = \frac{I^{\mathrm{MSHG}}(\mathrm{on},\,\Delta t) - I^{\mathrm{MSHG}}(\mathrm{off})}{I^{\mathrm{MSHG}}(\mathrm{off})}$. The data were taken at 77 K on EuO doped with 2.65% Gd (T_C ~119 K). The excitation density of the linearly polarized pump pulse is $\sim$380 μJ/cm^2. Following the photoexcitation at $\Delta t = 0$, a continuous increase of the MSHG intensity up to +30% at 3 ps is observed. This is followed by a continuous decrease passing zero at 40 ps and −25% at 3 ns.

On the basis of the results, the photoinduced increase and decrease of the MSHG intensity can be explained as follows. First, as is clear from the temperature dependence of $\sqrt{I^{\mathrm{MSHG}}}$ in Figure 4b, which reflects that of magnetization, before photoexcitation the direction of localized $4f$ spins is not fully aligned at 77 K due to a relatively high temperature (left panel in Figure 5b). When this magnetic state is irradiated with pump pulse, the excited 5*d* electrons spread to the adjacent Eu sites, and the thermally fluctuating localized $4f$ spins are partly aligned ferromagnetically through the intra-atomic $4f$–$5d$ exchange interaction, which leads to the increase of macroscopic magnetization

($\Delta M > 0$) (middle panel in Figure 5b). Considering that the energy of the intra-atomic $4f$–$5d$ exchange interaction is ~0.1 eV [32], which corresponds to a time of ~40 fs, an instantaneous increase of the MSHG intensity after the photoexcitation might be expected in contrast to the strikingly different time of ~3 ps. We have, however, to take into account that the magnetic exchange coupling is mediated via the RKKY interaction. The time τ_0 required to coherently establish its enhancement in the photoexcited region can be estimated from the time it takes the electronic correlation to spread through the crystal. The relevant distance is the RKKY wavelength, and the propagation velocity is the group velocity of the magnetic exciton. The latter is reduced with respect to the conduction electron group velocity by the ratio m_e^*/m_h^* of the effective masses of the $5d/6s$ conduction electrons (m_e^*) and of the heavy holes in the $4f$ band (m_h^*), which together form the magnetic exciton. The ratio m_h^*/m_e^* was taken to be equal to the inverse ratio of the respective bandwidths and was extracted from literature data [52] to be $\sim 4 \times 10^3$. In addition, the low excitation energy within the conduction band of $\Delta E \sim 0.5$ eV and the small wavenumber associated to this energy allows us to assume the conduction band as parabolic. Here, ΔE is the difference between the pump photon energy $\hbar\omega_{\mathrm{pump}}$ and the $4f$–$5d/6s$ gap energy E_{gap}. With $\tau_0 = \frac{h}{4\Delta E} \cdot \frac{m_h^*}{m_e^*}$ we thus obtain a build-up time τ_0 of ~8 ps, which is in reasonable agreement with the measured value of ~3 ps.

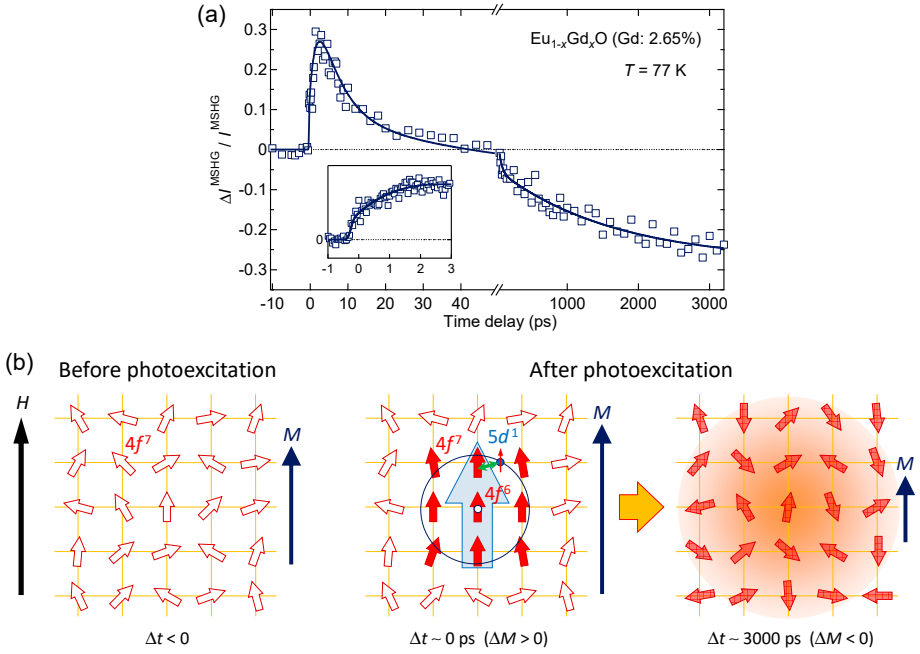

Figure 5. (**a**) Time evolution of the photoinduced change of the MSHG intensity normalized by the value before optical excitation, $\Delta I^{\mathrm{MSHG}}/I^{\mathrm{MSHG}}$ at 77 K for EuO doped with 2.65% Gd. The excitation density of the pump pulse is ~380 μJ/cm^2. The inset shows a magnified view of the ultrafast increase of the MSHG signal. Solid lines are guides to the eyes. (**b**) Schematics of ultrafast alignment of localized $4f^7$ spins by resonant $4f$–$5d$ photoexcitation and subsequent demagnetization processes.

The ensuing decrease of MSHG intensity on the ns timescale is associated with the demagnetization ($\Delta M < 0$) by the heating of the spin system through the transfer of the optical excitation energy from the electron system to the lattice and the spins (right panel in Figure 5b). The observed slow relaxation is consistent with the empirical thermal demagnetization time [53] inferred from the magnetocrystalline anisotropy constant of EuO [54], and the decrease of the MSHG intensity is consistent with the laser-pulse heating calculated from the absorption coefficient and the heat capacity of EuO [55].

3.3.2. Carrier-Density-Dependent Ultrafast Spin Dynamics

Having interpreted a microscopic model of photoinduced spin dynamics at a relatively high temperature, the question now is how much the magnitude of the magnetic interaction has changed by the photoexcitation and how is the relationship between the spin dynamics and the carrier density n_c. To simplify this investigation, the corresponding dynamics were measured at 10 K where the magnetic moment is fully saturated at 7 μ_B per Eu^{2+} ion. Hence, referring to relation (3), the nonthermal changes of the MSHG intensity is associated to the changes of J_{ex}.

Figure 6 shows the time evolution of the photoinduced changes of the MSHG intensity at 10 K for Gd concentrations between 0.013% and 19.5%. The excitation density of the pump pulse is ~130 μJ/cm^2 for all traces, which roughly corresponds to $\Delta n_c \sim 1 \times 10^{19}$ cm^{-3} carriers excited by photoexcitation. A common behavior observed for all samples is the decreasing MSHG intensity on a ns timescale. As mentioned above, this is caused by the thermal destabilization of the magnetic order mediated by the spin-lattice relaxation. A prolonged positive signal ($\Delta I^{MSHG}/I^{MSHG} > 0$), especially observed for $x = 0.25\%$, is related to the stability of photoenhanced ferromagnetic state, as described below. The MSHG response on the ps timescale strongly depends on the Gd concentration. At the lowest doping ($x = 0.013\%$), an ultrafast increase of the MSHG signal is observed. It nicely confirms that our nonlinear magneto-optical probe reflects a variation of J_{ex} rather than that of the already saturated magnetization. By increasing the Gd concentration, the magnitude of this initial increase becomes progressively more pronounced and reaches a maximum near $x = 0.25\%$. Higher Gd doping reduces the magnitude of the initial enhancement, and at $x > 5\%$ an ultrafast decrease of the MSHG signal is observed.

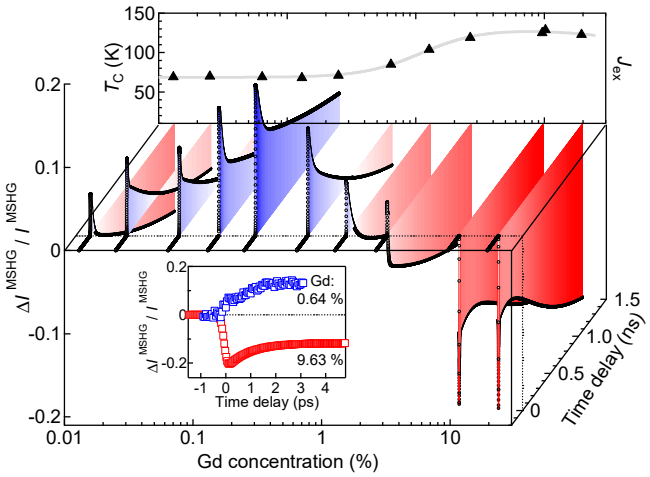

Figure 6. Change of the MSHG intensity at 10 K in $Eu_{1-x}Gd_xO$ as a function of time delay and Gd concentration (0.013% $\leq x \leq$ 19.5%). The excitation density of the pump pulse is ~130 μJ/cm^2 for all traces, which creates a photo-carrier density $\Delta n_c \sim 1 \times 10^{19}$ cm^{-3}. The inset shows a magnified view of the ultrafast increase and decrease of the MSHG intensity for $x = 0.64\%$ and $x = 9.63\%$.

In order to illustrate this behavior, in Figure 7a the pump-induced change of the MSHG intensity $\Delta I^{MSHG}/I^{MSHG}$ at the fixed time delay $\Delta t = 3$ ps is plotted as a function of Gd-dependent carrier density n_c. Here, n_c has been derived for each Gd concentration x from the relation displayed in the inset of Figure 3b. When the photoinduced change in the magnetization M is neglected, the relationship of $\Delta I^{MSHG}/I^{MSHG} = 2\Delta J_{ex}/J_{ex}$ is established from the relation (3). To obtain insight into this relation, it should be clarified how the photoinduced population of the $5d/6s$ band affects J_{ex}. Figure 7b shows $\Delta J_{ex}/J_{ex}$ obtained by increasing the equilibrium carrier density n_c of the $5d/6s$ band by a fixed value $\Delta n_c \sim 1 \times 10^{19}$ cm^{-3} which represents the photo-carrier density injected by the pump pulse in this experiment. The relation between $\Delta J_{ex}/J_{ex}$ and Δn_c was derived by the relation between T_C and n_c in Figure 3b, assuming that J_{ex} is simply proportional to T_C ($\Delta J_{ex}/J_{ex} = \Delta T_C/T_C$). For low

values of n_c, Δn_c simply set the net carrier density to 1×10^{19} cm^{-3} which results in a constant shift of ΔJ_{ex}. For high values of n_c the increase of the net carrier density by Δn_c is negligible, and so is ΔJ_{ex}. A pronounced change is observed at $n_c \sim 1 \times 10^{19}$ cm^{-3}, where the magnitude of the exchange interaction is very sensitive to the change in the carrier density (Figure 3b). Figure 7b reveals that the enhancement of J_{ex} exceeds an impressive 10% in this region and well reproduces the experimental results for $n_c \lesssim 10^{20}$ cm^{-3}, and thus the characteristic increase of the MSHG intensity in Figure 7a is closely related to the increase in the exchange interaction J_{ex} caused by the introduction of photoexcited carriers.

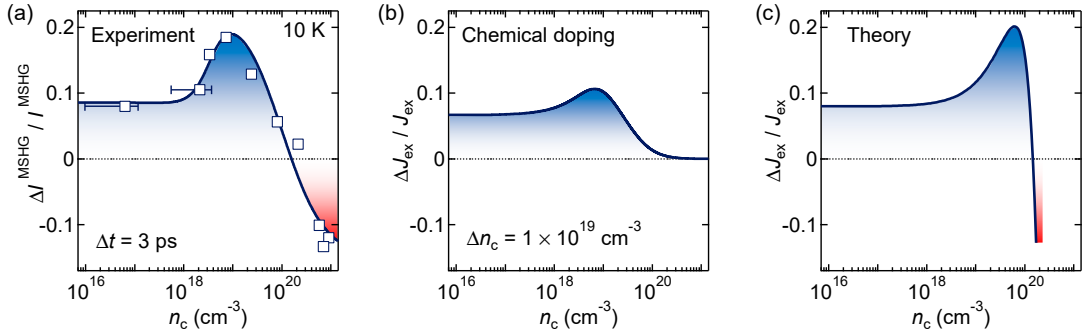

Figure 7. Optical tuning of the exchange interaction J_{ex} in carrier-density-controlled ferromagnetic semiconductor $Eu_{1-x}Gd_xO$. (**a**) Relation between n_c and the photoinduced change of the MSGH intensity at $\Delta t = 3$ ps and at 10 K, extracted from the experiments in Figure 6. (**b**) Calculated result of $\Delta J_{ex}/J_{ex}$ by adding a photoinduced carrier density $\Delta n_c = 1 \times 10^{19}$ cm^{-3} to the Gd-dependent carrier density n_c of the conduction band. Here, $\Delta J_{ex}/J_{ex}$ was calculated using the curve in Figure 3b, assuming that J_{ex} is simply proportional to T_C ($\Delta J_{ex}/J_{ex} = \Delta T_C/T_C$). (**c**) Theoretical calculation of $\Delta J_{ex}/J_{ex}$ based on the modification of the RKKY interaction by the photoinduced non-equilibrium population of the $5d/6s$ conduction band.

4. Discussion

The observed carrier-density-dependent ultrafast spin dynamics can be explained more qualitatively as follows. In the low-doped $Eu_{1-x}Gd_xO$ the carrier thermalization time is much longer than the one in dense itinerant ferromagnets like Ni or Gd. Charge thermalization is slow because it occurs by electron–electron scattering, the rate of which is proportional to carrier concentration. In low-doped $Eu_{1-x}Gd_xO$, the carrier concentration is by a factor of about 100 lower than that in pure Gd. The carrier thermalization time in pure Gd equals 50–100 fs [56]. With this, the factor of 100 leads to a prolonged carrier thermalization time of low-doped $Eu_{1-x}Gd_xO$ of 5–10 ps. It is therefore concluded that the dynamics for the first few ps is dominated by a non-equilibrium charge carrier distribution, that is, the three-temperature model (3TM) [57], where the coupled electron, spin and lattice subsystems are each assumed to be in equilibrium at their respective temperatures, is not applicable. Hence, for the first few ps after the photoexcitation, the $4f$ electron population, which is photoexcited into the state with $5d$ electron character, contributes to a stronger magnetic coupling between the Eu $4f$ spins. This coupling mechanism is in agreement with the experimental observations on the low-doped samples.

On the other hand, as shown in Figure 7b, it does not explain the photoinduced decrease of the MSHG intensity in the region where the carrier density is sufficiently high ($n_c \sim 1 \times 10^{21}$ cm^{-3}). In the picture of the 3TM, the optical pump pulse would, in addition to exciting the localized $4f$ electrons and creating the $4f^6 5d(t_{2g})$ magnetic excitons, lead to the excitation of the chemically doped carriers in the $5d/6s$ conduction band and to their thermalization at the elevated temperature corresponding to the deposited energy. This would invariably reduce J_{ex} since the ferromagnetic coupling with electrons in the energetically higher band states becomes weaker because of their

increased wavenumber. Furthermore, the increased temperature would directly contribute to the demagnetization.

As shown in Ref. [52], an increase in the carrier density in the conduction band by chemical or photo-doping strengthens its interaction with the Gd impurity band. This entails an energetic downshift of the conduction band toward the Gd impurity band and, hence, a reduction of the $4f$–$5d/6s$ gap energy. This shift affects the $4f$–$4f$ RKKY exchange. Using the many-body renormalization theory introduced in Ref. [52], the RKKY-like coupling for the non-equilibrium electron distribution was calculated. The resultant $\Delta J_{ex}/J_{ex}$ is plotted in Figure 7c as a function of the carrier density n_c. According to the theory, the non-monotonic behaviors in Figure 7a,c can be understood as follows. The density of photoexcited carriers is proportional to the spectral density at the energy $\hbar\omega_{pump} - E_{gap}$ addressed by the photoexcitation. Therefore, as E_{gap} is reduced with increasing Gd doping and, thus, increasing n_c, more states can be populated with photoexcited carriers. The enhanced density of excited carriers contributes to the increase of $\Delta J_{ex}/J_{ex}$ with n_c. In contrast, for $n_c > 10^{20}$ cm^{-3}, $\Delta J_{ex}/J_{ex}$ and $\Delta I^{MSHG}/I^{MSHG}$ get quenched to negative values for two reasons. First, with further downward shift of the conduction band the energy mismatch $\hbar\omega_{pump} - E_{gap}$, and with it the wavenumber of the photoexcited carriers, increases further. Thus, because of the oscillating dependence of the RKKY coupling on the wavenumber, J_{ex} turns over towards weaker ferromagnetic coupling. Second, with the increasingly metallic nature, the electron–electron scattering time gets reduced, leading to ultrafast thermalization and concomitant magnetization quenching, that is, conventional demagnetization according to the 3TM begins to dominate. This is nicely reflected by the change of the build-up time from ~3 ps (manifestation of RKKY interaction) to ~100 fs (thermalization according to the 3TM) in the inset of Figure 6.

Finally, I will show the continuous tuning of the exchange interaction is possible by changing the excitation density of the pump pulse. Figure 8a shows the excitation density dependence of the change of the MSHG intensity at $\Delta t = 3$ ps and at 10 K for selected Gd concentrations. Apart from the result for $x = 10.2\%$, where the decrease of $\Delta I^{MSHG}/I^{MSHG}$ due to the ultrafast demagnetization is observed, the overall tendencies are roughly consistent with those of $\Delta J_{ex}/J_{ex}$ plotted in Figure 8b as a function of the additional carrier density Δn_c. Here, the Δn_c dependence of $\Delta J_{ex}/J_{ex}$ was calculated by increasing the equilibrium carrier density n_c of the $5d/6s$ band for each Gd concentration. The largest enhancement of $\Delta J_{ex}/J_{ex}$ is seen for $x = 0.25\%$ because J_{ex} is very sensitive to the change of n_c in this doping region. This result corroborates the above discussion and provides a possibility to control the exchange interaction on the sub-ps timescale in a well-controlled way.

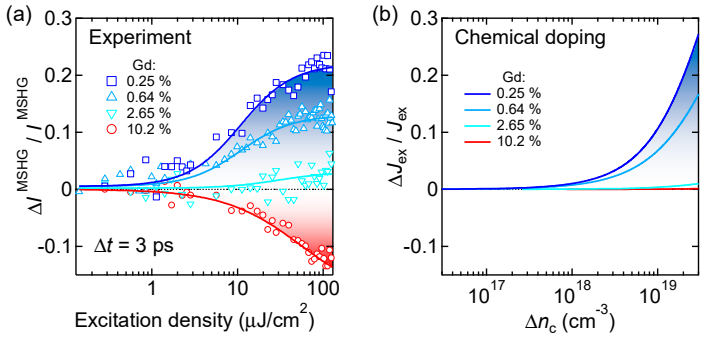

Figure 8. Continuous optical tuning of the exchange interaction J_{ex} in ferromagnetic semiconductor $Eu_{1-x}Gd_xO$. (**a**) Excitation density dependence of the change of the MSHG intensity at $\Delta t = 3$ ps and at 10 K for selected Gd concentrations. Solid lines are guides to the eyes. (**b**) Calculated result of the Δn_c dependence of $\Delta J_{ex}/J_{ex}$. Here, $\Delta J_{ex}/J_{ex}$ was calculated using the curve in Figure 3b, assuming that J_{ex} is simply proportional to T_C ($\Delta J_{ex}/J_{ex} = \Delta T_C/T_C$).

5. Conclusions

In this review paper, I showed that ultrafast magnetic coupling dynamics can be tuned from photoinduced enhancement to photoinduced quenching of ferromagnetic order in carrier-density-controlled ferromagnetic semiconductor $Eu_{1-x}Gd_xO$. The largest enhancement of the ferromagnetic order and the crossover to quenching were observed around $n_c \sim 10^{19}$ cm^{-3} and $\sim 10^{20}$ cm^{-3}, respectively. These behaviors are explained by a non-equilibrium theory that extends beyond the established 3TM. In contrast to systems with a high carrier concentration like transition-metal, rare-earth or certain diluted-magnetic-semiconductor ferromagnets, the sub-ps carrier dynamics in low-doped $Eu_{1-x}Gd_xO$ is far from equilibrium due to a substantially longer electron thermalization time. Our experimental results and their theoretical modelling not only demonstrate how to control the stability of a ferromagnetic state on the ultrafast timescale, but also give a guide to the material selection and design for the dynamical optical control of magnetic interactions: systems with a low density of conduction band carriers (which is tunable) but with a high density of magnetic moments (unlike, for example, in diluted magnetic semiconductors) are favorable candidates. Further advances in both experimental and theoretical fields will provide a bright future for ultrafast spintronics applications.

Funding: This work was supported by JSPS KAKENHI (Grant No. 17H04844), Research Foundation for Opto-Science and Technology, the Alexander von Humboldt Foundation, the SNSF (Grant No. 200021_147080/1), the TRR 80 of the DFG and the AFOSR (Grant No. FA9550-10-1-0123).

Acknowledgments: The author would like to thank A. Schroer, A. Schmehl, A. Melville, C. Becher, M. Trujillo-Martinez, D. G. Schlom, J. Mannhart, J. Kroha, and M. Fiebig for experimental help and fruitful discussions.

Conflicts of Interest: The author declares no conflict of interest.

References

1. Wolf, S.A.; Awschalom, D.D.; Buhrman, R.A.; Daughton, J.M.; von Molnár, S.; Roukes, M.L.; Chtchelkanova, A.Y.; Treger, D.M. Spintronics: A spin-based electronics vision for the future. *Science* **2001**, *294*, 1488–1495. [CrossRef] [PubMed]
2. Kirilyuk, A.; Kimel, A.V.; Rasing, T. Ultrafast optical manipulation of magnetic order. *Rev. Mod. Phys.* **2010**, *82*, 2731–2784. [CrossRef]
3. Beaurepaire, E.; Merle, J.-C.; Daunois, A.; Bigot, J.-Y. Ultrafast spin dynamics in ferromagnetic nickel. *Phys. Rev. Lett.* **1996**, *76*, 4250–4253. [CrossRef] [PubMed]
4. Hohlfeld, J.; Matthias, E.; Knorren, R.; Bennemann, K.H. Nonequilibrium magnetization dynamics of nickel. *Phys. Rev. Lett.* **1997**, *78*, 4861–4864. [CrossRef]
5. Scholl, A.; Baumgarten, L.; Jacquemin, R.; Eberhardt, W. Ultrafast spin dynamics of ferromagnetic thin films observed by fs spin-resolved two-photon photoemission. *Phys. Rev. Lett.* **1997**, *79*, 5146–5149. [CrossRef]
6. Koopmans, B.; van Kampen, M.; Kohlhepp, J.T.; de Jonge, W.J.M. Ultrafast magneto-optics in nickel: Magnetism or optics? *Phys. Rev. Lett.* **2000**, *85*, 844–847. [CrossRef] [PubMed]
7. Stanciu, C.D.; Hansteen, F.; Kimel, A.V.; Kirilyuk, A.; Tsukamoto, A.; Itoh, A.; Rasing, T. All-optical magnetic recording with circularly polarized light. *Phys. Rev. Lett.* **2007**, *99*, 047601. [CrossRef] [PubMed]
8. Radu, I.; Vahaplar, K.; Stamm, C.; Kachel, T.; Pontius, N.; Dürr, H.A.; Ostler, T.A.; Barker, J.; Evans, R.F.L.; Chantrell, R.W.; et al. Transient ferromagnetic-like state mediating ultrafast reversal of antiferromagnetically coupled spins. *Nature* **2011**, *472*, 205–208. [CrossRef] [PubMed]
9. Koshihara, S.; Munekata, H. Ferromagnetic order induced by photogenerated carriers in magnetic III-V semiconductor heterostructures of (In,Mn)As/GaSb. *Phys. Rev. Lett.* **1997**, *78*, 4617–4620. [CrossRef]
10. Wang, J.; Cotoros, I.; Dani, K.M.; Liu, X.; Furdyna, J.K.; Chemla, D.S. Ultrafast enhancement of ferromagnetism via photoexcited holes in GaMnAs. *Phys. Rev. Lett.* **2007**, *98*, 217401. [CrossRef] [PubMed]
11. Matsubara, M.; Okimoto, Y.; Ogasawara, T.; Tomioka, Y.; Okamoto, H.; Tokura, Y. Ultrafast photoinduced insulator-ferromagnet transition in the perovskite manganite $Gd_{0.55}Sr_{0.45}MnO_3$. *Phys. Rev. Lett.* **2007**, *99*, 207401. [CrossRef] [PubMed]
12. Satoh, T.; Terui, Y.; Moriya, R.; Ivanov, B.A.; Ando, K.; Saitoh, E.T. Shimura, and K Kuroda: Directional control of spin-wave emission by spatially shaped light. *Nat. Photonics* **2012**, *6*, 662–666. [CrossRef]

13. Matsubara, M.; Schroer, A.; Schmehl, A.; Melville, A.; Becher, C.; Trujillo-Martinez, M.; Schlom, D.G.; Mannhart, J.; Kroha, J.; Fiebig, M. Ultrafast optical tuning of ferromagnetism via the carrier density. *Nat. Commun.* **2015**, *6*, 6724. [CrossRef] [PubMed]
14. Matthias, B.T.; Bozorth, R.M.; Van Vleck, J.H. Ferromagnetic interaction in EuO. *Phys. Rev. Lett.* **1961**, *7*, 160–161. [CrossRef]
15. Mauger, A.; Godart, C. The magnetic, optical, and transport properties of representatives of a class of magnetic semiconductors: The europium chalcogenides. *Phys. Rep.* **1986**, *141*, 51–176. [CrossRef]
16. Schoenes, J.; Wachter, P. Exchange optics in Gd-doped EuO. *Phys. Rev. B* **1974**, *9*, 3097–3105. [CrossRef]
17. Steeneken, P.G.; Tjeng, L.H.; Elfimov, I.; Sawatzky, G.A.; Ghiringhelli, G.; Brookes, N.B.; Huang, D.-J. Exchange splitting and charge carrier spin polarization in EuO. *Phys. Rev. Lett.* **2002**, *88*, 047201. [CrossRef] [PubMed]
18. Santos, T.S.; Moodera, J.S.; Raman, K.V.; Negusse, E.; Holroyd, J.; Dvorak, J.; Liberati, M.; Idzerda, Y.U.; Arenholz, E. Determining exchange splitting in a magnetic semiconductor by spin-filter tunneling. *Phys. Rev. Lett.* **2008**, *101*, 147201. [CrossRef] [PubMed]
19. Petrich, G.; von Molnár, S.; Penney, T. Exchange-induced autoionization in Eu-rich EuO. *Phys. Rev. Lett.* **1971**, *26*, 885–888. [CrossRef]
20. Oliver, M.R.; Dimmock, J.O.; McWhorter, A.L.; Reed, T.B. Conductivity studies in europium oxide. *Phys. Rev. B* **1972**, *5*, 1078–1098. [CrossRef]
21. Shapira, Y.; Foner, S.; Reed, T.B. EuO. I. Resistivity and Hall effect in fields up to 150 kOe. *Phys. Rev. B* **1973**, *8*, 2299–2315. [CrossRef]
22. Ahn, K.Y.; Shafer, M.W. Relationship between stoichiometry and properties of EuO films. *J. Appl. Phys.* **1970**, *41*, 1260–1262. [CrossRef]
23. Wang, H.-Y.; Schoenes, J.; Kaldis, E. Magneto-optical polar Kerr efffect of EuO. *Helv. Phys. Acta* **1986**, *59*, 102–105.
24. Matsubara, M.; Schmehl, A.; Mannhart, J.; Schlom, D.G.; Fiebig, M. Large nonlinear magneto-optical effect in the centrosymmetric ferromagnetic semiconductor EuO. *Phys. Rev. B* **2010**, *81*, 214447. [CrossRef]
25. Matsubara, M.; Becher, C.; Schmehl, A.; Mannhart, J.; Schlom, D.G.; Fiebig, M. Optical second- and third-harmonic generation on the ferromagnetic semiconductor europium oxide. *J. Appl. Phys.* **2011**, *109*, 07C309. [CrossRef]
26. Matsubara, M.; Schmehl, A.; Mannhart, J.; Schlom, D.G.; Fiebig, M. Giant third-order magneto-optical rotation in ferromagnetic EuO. *Phys. Rev. B* **2012**, *86*, 195127. [CrossRef]
27. Bousquet, E.; Spaldin, N.A.; Ghosez, P. Strain-induced ferroelectricity in simple rocksalt binary oxides. *Phys. Rev. Lett.* **2010**, *104*, 037601. [CrossRef] [PubMed]
28. Schmehl, A.; Vaithyanathan, V.; Herrnberger, A.; Thiel, S.; Richter, C.; Liberati, M.; Heeg, T.; Röckerath, M.; Kourkoutis, L.F.; Mühlbauer, S.; et al. Epitaxial integration of the highly spin-polarized ferromagnetic semiconductor EuO with silicon and GaN. *Nat. Mater.* **2007**, *6*, 882–887. [CrossRef] [PubMed]
29. Ulbricht, R.W.; Schmehl, A.; Heeg, T.; Schubert, J.; Schlom, D.G. Adsorption-controlled growth of EuO by molecular-beam epitaxy. *Appl. Phys. Lett.* **2008**, *93*, 102105. [CrossRef]
30. Swartz, A.G.; Ciraldo, J.; Wong, J.J.I.; Li, Y.; Han, W.; Lin, T.; Mack, S.; Shi, J.; Awschalom, D.D.; Kawakami, R.K. Epitaxial EuO thin films on GaAs. *Appl. Phys. Lett.* **2010**, *97*, 112509. [CrossRef]
31. Mairoser, T.; Schmehl, A.; Melville, A.; Heeg, T.; Canella, L.; Böni, P.; Zander, W.; Schubert, J.; Shai, D.E.; Monkman, E.J.; et al. Is there an intrinsic limit to the charge-carrier-induced increase of the Curie temperature of EuO? *Phys. Rev. Lett.* **2010**, *105*, 257206. [CrossRef] [PubMed]
32. Kasuya, T. s-f exchange interactions and magnetic semiconductors. *CRC Crit. Rev. Solid State Sci.* **1972**, *3*, 131–164. [CrossRef]
33. Ott, H.; Heise, S.J.; Sutarto, R.; Hu, Z.; Chang, C.F.; Hsieh, H.H.; Lin, H.-J.; Chen, C.T.; Tjeng, L.H. Soft x-ray magnetic circular dichroism study on Gd-doped EuO thin films. *Phys. Rev. B* **2006**, *73*, 094407. [CrossRef]
34. Desfours, J.P.; Nadai, J.P.; Averous, M.; Godard, G. Light induced molecular magnetic polaron in EuO. *Solid State Commun.* **1976**, *20*, 691–694. [CrossRef]
35. Liu, F.; Makino, T.; Yamasaki, T.; Ueno, K.; Tsukazaki, A.; Fukumura, T.; Kong, Y.; Kawasaki, M. Ultrafast time-resolved Faraday rotation in EuO thin films. *Phys. Rev. Lett.* **2012**, *108*, 257401. [CrossRef] [PubMed]
36. Makino, T.; Liu, F.; Yamasaki, T.; Kozuka, Y.; Ueno, K.; Tsukazaki, A.; Fukumura, T.; Kong, Y.; Kawasaki, M. Ultrafast optical control of magnetization in EuO thin films. *Phys. Rev. B* **2012**, *86*, 064403. [CrossRef]

37. Pavlov, V.V.; Pisarev, R.V.; Nefedov, S.G.; Akimov, I.A.; Yakovlev, D.R.; Bayer, M.; Henriques, A.B.; Rappl, P.H.O.; Abramof, E. Magnetic-field-induced crossover from the inverse Faraday effect to the optical orientation in EuTe. *J. Appl. Phys.* **2018**, *123*, 193102. [CrossRef]
38. Subkhangulov, R.R.; Henriques, A.B.; Rappl, P.H.O.; Abramof, E.; Rasing, T.; Kimel, A.V. All-optical manipulation and probing of the d–f exchange interaction in EuTe. *Sci. Rep. B* **2014**, *4*, 4368. [CrossRef] [PubMed]
39. Hohlfeld, J.; Conrad, U.; Matthias, E. Does femtosecond time-resolved second-harmonic generation probe electron temperatures at surfaces? *Appl. Phys. B Lasers Opt.* **1996**, *63*, 541–544. [CrossRef]
40. Melnikov, A.; Radu, I.; Bovensiepen, U.; Krupin, O.; Starke, K.; Matthias, E.; Wolf, M. Coherent optical phonons and parametrically coupled magnons induced by femtosecond laser excitation of the Gd(0001) surface. *Phys. Rev. Lett.* **2003**, *91*, 227403. [CrossRef] [PubMed]
41. Duong, N.P.; Satoh, T.M.; Fiebig, M. Ultrafast manipulation of antiferromagnetism of NiO. *Phys. Rev. Lett.* **2004**, *93*, 117402. [CrossRef] [PubMed]
42. Matsubara, M.; Kaneko, Y.; He, J.-P.; Okamoto, H.; Tokura, Y. Ultrafast polarization and magnetization response of multiferroic $GaFeO_3$ using time-resolved nonlinear optical techniques. *Phys. Rev. B* **2009**, *79*, 140411. [CrossRef]
43. Shen, Y.R. *The Principles of Nonlinear Optics*; John Wiley & Sons: New York, NY, USA, 1984; ISBN 10 0471430803.
44. Bennemann, K.H. *Nonlinear Optics in Metals*; Clarendon Press: Oxford, UK, 1998; ISBN 10 0198518935.
45. Fiebig, M.; Pavlov, V.V.; Pisarev, R.V. Second-harmonic generation as a tool for studying electronic and magnetic structures of crystals: Review. *J. Opt. Soc. Am. B* **2005**, *22*, 96–118. [CrossRef]
46. Birss, R.R. *Symmetry and Magnetism*; North-Holland: Amsterdam, The Netherlands, 1966; ISBN 10 0720414539.
47. Fiebig, M.; Fröhlich, D.; Lottermoser, T.; Pavlov, V.V.; Pisarev, R.V.; Weber, H.-J. Second harmonic generation in the centrosymmetric antiferromagnet NiO. *Phys. Rev. Lett.* **2001**, *87*, 137202. [CrossRef] [PubMed]
48. Kaminski, B.; Lafrentz, M.; Pisarev, R.V.; Yakovlev, D.R.; Pavlov, V.V.; Lukoshkin, V.A.; Henriques, A.B.; Springholz, G.; Bauer, G.; Abramof, E.; et al. Spin-induced optical second harmonic generation in the centrosymmetric magnetic semiconductors EuTe and EuSe. *Phys. Rev. Lett.* **2009**, *103*, 057203. [CrossRef] [PubMed]
49. Kaminski, B.; Lafrentz, M.; Pisarev, R.V.; Yakovlev, D.R.; Pavlov, V.V.; Lukoshkin, V.A.; Henriques, A.B.; Springholz, G.; Bauer, G.; Abramof, E.; et al. Optical second harmonic generation in the centrosymmetric magnetic semiconductors EuTe and EuSe. *Phys. Rev. B* **2010**, *81*, 155201. [CrossRef]
50. Henriques, A.B.; Abramof, E.; Rappl, P.H.O. Theory of near-gap second harmonic generation in centrosymmetric magnetic semiconductors: Europium chalcogenides. *Phys. Rev. B* **2009**, *80*, 245206. [CrossRef]
51. Freiser, M.J.; Holtzberg, F.; Methfessel, S.; Pettit, G.D.; Shafer, M.W.; Suits, J.C. The magnetic red shift in europium chalcogenides. *Helv. Phys. Acta* **1968**, *41*, 832–838.
52. Arnold, M.; Kroha, J. Simultaneous ferromagnetic metal-semiconductor transition in electron-doped EuO. *Phys. Rev. Lett.* **2008**, *100*, 046404. [CrossRef] [PubMed]
53. Ogasawara, T.; Ohgushi, K.; Tomioka, Y.; Takahashi, K.S.; Okamoto, H.; Kawasaki, M.; Tokura, Y. General features of photoinduced spin dynamics in ferromagnetic and ferrimagnetic compounds. *Phys. Rev. Lett.* **2005**, *94*, 087202. [CrossRef] [PubMed]
54. Miyata, N.; Argyle, B.E. Magnetocrystalline anisotropy of single-crystal europium oxide. *Phys. Rev.* **1967**, *157*, 448–451. [CrossRef]
55. Ahn, K.; Pecharsky, A.O.; Gschneidner, K.A., Jr.; Pecharsky, V.K. Preparation, heat capacity, magnetic properties, and the magnetocaloric effect of EuO. *J. Appl. Phys.* **2004**, *97*, 063901. [CrossRef]
56. Wietstruk, M.; Melnikov, A.; Stamm, C.; Kachel, T.; Pontius, N.; Sultan, M.; Gahl, C.; Weinelt, M.; Durr, H.A.; Bovensiepen, U. Hot-electron-driven enhancement of spin-lattice coupling in Gd and Tb *4f* ferromagnets observed by femtosecond X-ray magnetic circular dichroism. *Phys. Rev. Lett.* **2011**, *106*, 127401. [CrossRef] [PubMed]
57. Koopmans, B.; Malinowski, G.; Dalla Longa, F.; Steiauf, D.; Fähnle, M.; Roth, T.; Cinchetti, M.; Aeschlimann, M. Explaining the paradoxical diversity of ultrafast laser-induced demagnetization. *Nat. Mater.* **2010**, *9*, 259–265. [CrossRef] [PubMed]